HHS Public Access

Author manuscript

Hippocampus. Author manuscript; available in PMC 2020 February 01.

Published in final edited form as:

Hippocampus. 2019 February ; 29(2): 78–92. doi:10.1002/hipo.23012.

Diversity of dendritic morphology and entorhinal cortex synaptic effectiveness in mouse CA2 pyramidal neurons

Thomas D. Helton[1], **Meilan Zhao**[1], **Shannon Farris**[1], and **Serena M. Dudek**[1]

[1]Neurobiology Laboratory, National Institute of Environmental Health Sciences, National Institutes of Health, 111 TW Alexander Drive, Mail Drop F2-04, Research Triangle Park, North Carolina 27709, USA

Abstract

Excitatory synaptic inputs from specific brain regions are often targeted to distinct dendritic arbors on hippocampal pyramidal neurons. Recent work has suggested that CA2 pyramidal neurons respond robustly and preferentially to excitatory input into the *stratum lacunosum moleculare* (SLM), with a relatively modest response to Schaffer collateral excitatory input into *stratum radiatum* (SR) in acute mouse hippocampal slices, but the extent to which this difference may be explained by morphology is unknown. In an effort to replicate these findings and to better understand the role of dendritic morphology in shaping responses from proximal and distal synaptic sites, we measured excitatory postsynaptic currents and action potentials in CA2 pyramidal cells in response to SR and SLM stimulation and subsequently analyzed confocal images of the filled cells. We found that, in contrast to previous reports, SR stimulation evoked substantial responses in all recorded CA2 pyramidal cells. Strikingly, however, we found that not all neurons responded to SLM stimulation, and in those neurons that did, responses evoked by SLM and SR were comparable in size and effectiveness in inducing action potentials. In a comprehensive morphometric analysis of CA2 pyramidal cell apical dendrites, we found that the neurons that were unresponsive to SLM stimulation were the same ones that lacked substantial apical dendritic arborization in the SLM. Neurons responsive to both SR and SLM stimulation had roughly equal amounts of dendritic branching in each layer. Remarkably, our study in mouse CA2 generally replicates the work characterizing the diversity of CA2 pyramidal cells in the guinea pig hippocampus. We conclude, then, that like in guinea pig, mouse CA2 pyramidal cells have a diverse apical dendrite morphology that is likely to be reflective of both the amount and source of excitatory input into CA2 from the entorhinal cortex and CA3.

Keywords

Apical dendrite; stratum radiatum; stratum lacunosum moleculare; EPSC; action potential

CORRESPONDING AUTHOR: Serena M. Dudek. National Institute of Environmental Health Sciences 111 TW Alexander Drive, Mail Drop F2-04, Research Triangle Park, North Carolina 27709, USA. (919) 287-3513. dudek@niehs.nih.gov.

Introduction:

In his 1934 study of the Cornus Ammonis (CA), Lorente de Nó subdivided the hippocampal cortex into four fields (CA1-CA4) based on morphological differences of the principal excitatory neurons, pyramidal cells, as well as on the specific connectivity between each field (Lorente de Nó, 1934). Recent work has shown that CA2 is indeed a separate hippocampal subregion that plays important roles in cognitive behaviors, including novelty detection (Alexander et al., 2016; Wintzer, Boehringer, Polygalov, & McHugh, 2014), social memory (Hitti & Siegelbaum, 2014; Pagani et al., 2015; Smith, Williams Avram, Cymerblit-Sabba, Song, & Young, 2016), and spatial coding (Alexander et al., 2016; Kay et al., 2016; S. A. Lee, Ferrari, Vallortigara, & Sovrano, 2015; Lu, Igarashi, Witter, Moser, & Moser, 2015; Mankin, Diehl, Sparks, Leutgeb, & Leutgeb, 2015; Oliva, Fernandez-Ruiz, Buzsaki, & Berenyi, 2016).

Pyramidal neurons in CA2 differ from those in CA1 and CA3 in excitatory input circuitry, synaptic plasticity, and protein expression (Cui, Gerfen, & Young, 2013; Dudek, Alexander, & Farris, 2016). They receive selective and prominent excitatory inputs from the supramammillary nucleus of the hypothalamus (SuM) (Borhegyi & Leranth, 1997; Kocsis & Vertes, 1994; Magloczky, Acsady, & Freund, 1994), and like CA3, a direct excitatory drive from the entorhinal cortex (EC), primarily from cells in layer II (Chevaleyre & Siegelbaum, 2010; Kohara et al., 2014; Srinivas et al., 2017). Interestingly, CA2 pyramidal neurons were reported to have an atypically strong excitation response to ECII stimulation compared with ECIII inputs to CA1 (Sun, Srinivas, Sotayo, & Siegelbaum, 2014). This phenomenon has been attributed to more extensive dendritic branching of CA2 pyramidal neurons within the stratum lacunosum moleclulare (SLM) than CA1 neurons and to the presence of local dendritic sodium spikes in CA2 distal apical dendrites not found in distal apical dendrites of CA1 (Sun et al., 2014). Excitatory synapses onto CA2 pyramidal neurons in the stratum radiatum are also resistant to synaptic plasticity (long term potentiation, or LTP, and to some degree long term depression, or LTD) (M. Zhao, Choi, Obrietan, & Dudek, 2007) and display unique pharmacology in inhibitory synaptic plasticity (Leroy, Brann, Meira, & Siegelbaum, 2017; Nasrallah, Piskorowski, & Chevaleyre, 2015; Piskorowski & Chevaleyre, 2013). CA2 neurons also have distinct expression patterns for several proteins, such as purkinje cell protein 4 (PCP4) (X. Zhao et al., 2001), regulator of G-protein signaling 14 (RGS14) (S. E. Lee et al., 2010), and the cellular adhesion molecule Amigo2 (Lein, Callaway, Albright, & Gage, 2005; Lein et al., 2007). This molecular signature further distinguishes CA2 from neighboring CA1 and CA3 regions.

Finally, morphology of CA2 pyramidal neurons is distinct from neighboring CA1 and CA3 hippocampal subfields in rodents. As early as 1934, Lorente de Nó recognized the morphological diversity in pyramidal neurons between hippocampal subregions in a number of species (Lorente de Nó, 1934). In the late 20th century, a comprehensive morphometric analysis of dendritic organization of rat hippocampal pyramidal cells by Ishizuka et al. noted a number of characteristics that differentiated CA1, CA2, and CA3 pyramidal neurons, including total dendritic length, cell body size, 1° and 2° apical dendritic branching, and the absence of thorny excrescences in CA1 and CA2 (Ishizuka, Cowan, & Amaral, 1995). More recent findings by Li et al. and Sun et al. have shown that CA1 and CA3, respectively,

display a heterogeneous dendritic structure (Li et al., 2017; Sun et al., 2017). Interestingly, nearly two decades earlier, Bartesaghi and Ravasi identified four distinct subtypes of CA2 pyramidal cells (Ma, Mb, Mc, and B cells) in guinea pig CA2 based on 1° apical dendrite morphology (Bartesaghi & Ravasi, 1999), indicating that a particularly heterogeneous population of pyramidal neuron morphologies also exists in CA2.

The aim of this study was to determine whether neurons in mouse CA2 share the four morphologically distinct CA2 pyramidal cell subtypes observed in guinea pig. In addition, we further sought to identify functional variations that may result from the differential morphologies. Here we report that, like in guinea pig, mouse CA2 pyramidal cells can be separated into distinct subtypes based on a number of objective morphometric criteria. Furthermore, we determined that certain types of CA2 neurons receive both effective cortical and Schaffer collateral excitatory input while a portion of them notably lack appreciable excitatory drive from EC as measured with electrical stimulation in the SLM. These findings raise the question of whether the different CA2 pyramidal cell subtypes and the associated differences in excitatory input play distinct roles in CA2 function.

Materials and Methods:

Intracellular recordings and biocytin filling.

All experimental procedures were approved by the Animal Care and Use Committee of NIEHS and were in accordance with the National Institutes of Health Guidelines for care and use of animals. Hippocampal slices were prepared from Amigo2-GFP+ mice (MMRRC-UC Davis, Davis, CA) on C57BL/6J background at postnatal day 30–45. Under deep anesthesia with Fatal-Plus (Vortech Pharmaceuticals, Dearborn MI), animals were transcardially perfused with cold sucrose-substituted artificial cerebral spinal fluid (ACSF) containing (in mM) 10 NaCl, 195 sucrose, 2.5 KCl, 10 glucose, 25 $NaHCO_3$, 1.25 NaH_2PO_4, 2 Na-pyruvate, 7 $MgCl_2$, 0.5 $CaCl_2$ continuously bubbled with 95% O_2/5% CO_2 to achieve a pH of 7.4. Once perfused, animals were decapitated, and brains rapidly removed and submerged in the same high-sucrose ACSF prior to slicing. Brains were sliced in the coronal plane at a thickness of 300 μm using a Leica VT 1200S vibratome (Leica Biosystems, Buffalo Grove IL). Freshly cut slices were placed in a holding chamber in standard ACSF (in mM: 125 NaCl, 2.5 KCl, 20 *D*-glucose, 25 NaHCO3, 1.25 NaH_2PO_4, 2 Na-pyruvate, 2 $CaCl_2$, 2 $MgCl_2$ continuously bubbled with 95% O_2/ 5% CO_2 to maintain pH 7.4) at a temperature of 37°C. After cutting, slices were allowed to recover for 1½ hours as temperature was gradually returned to room temperature.

Whole-cell recordings were made from Amigo2-GFP-expressing CA2 neurons in the pyramidal cell layer using pipettes (3–5 MΩ resistance) filled with a solution containing the following (in mM): 135 K-gluconate, 5 KCl, 0.1 Na-EGTA, 10 HEPES, 2 NaCl, 5 Mg-ATP, 0.4 Na-GTP, 10 Na_2-phosphocreatine, 0.5% w/v biocytin (Sigma-Aldrich, St. Louis, MO) pH 7.2 HCl/KOH. Data were collected using either Clampex 10.6 or Patchmaster software and analyzed using Clampfit 10.6 or Fitmaster software (Molecular Devices, Sunnyvale, CA. Heka Instruments Inc. Holliston MA, respectively). Series and input resistances were monitored by measuring the response to a 10 mV step at each stimulation. The liquid junction potential was 10 mV, and membrane potentials reported were corrected accordingly.

Recordings were not compensated for series resistance. Stimulating electrodes (cluster-type) from FHC (Bowdoinham, ME) were used to evoke excitatory postsynaptic currents (EPSCs; in voltage clamp mode) or action potentials (in current clamp mode). Shaffer collateral-stimulating electrodes and perforant path stimulating electrodes were placed, in close proximity to CA2, in the CA3 side of the stratum radiatum (SR) and in the CA1 side of the stratum lacunosum moleculare (SLM). Responses were evoked with either a single pulse (for EPSCs, measured in voltage clamp mode from a holding potential of -60mV) or 5 pulses at 100 Hz (to induce action potentials, measured in current clamp mode) in an effort to match the conditions described by Sun, et al (Sun et al., 2014). Stimulus pulses in both cases were 200 microseconds in duration.

Immunohistochemistry.

Post-recording, brain slices were immediately transferred to 4% paraformaldehyde (PFA) in phosphate buffered saline (PBS) for fixation and incubated at room temperature for 2 hours. Post fixation, slices were washed three times for 5 minutes in PBS to remove residual PFA then blocked overnight at 4°C with gentle agitation in PBS containing 3% normal goat serum (NGS) and 0.3% Triton X100. Blocked slices were then transferred to 1° antibody solution (PBS with 3% NGS and 0.3% Triton X-100) containing either PCP-4 antibody (Santa Cruz Biotechnology, Dallas, TX) at 1:250 dilution or RGS-14 antibody (Antibodies Inc., Davis, CA) at 1:250 dilution and incubated for 2 days at 4°C with gentle agitation. Subsequently, slices were washed 3 X 10 minutes at room temperature in PBS/0.3% Triton X-100 and then transferred to 2° antibody solution (PBS with 3% NGS and 0.3% Triton X-100 containing either goat anti rabbit Alexa Fluor-conjugated 633 (PCP-4) or goat anti mouse Alexa Fluor-conjugated 633 (RGS-14) plus Alexa Fluor 488, 568, or 633 conjugated streptavidin; ThermoFisher, Waltham, MA) and incubated for 2 days at 4°C with gentle agitation. Slices were then washed 3 X 10 minutes in PBS/0.3% Triton X-100 with gentle agitation then transferred to PBS. Twenty minutes prior to imaging, slices were incubated in 60% 2,2'-thiodiethanol to clear the tissue (Aoyagi, Kawakami, Osanai, Hibi, & Nemoto, 2015) and then imaged on a Zeiss 880 laser scanning confocal microscope (Carl Zeiss AG, Oberkochen, Germany). Only CA2 pyramidal neurons, confirmed as either GFP positive or located among PCP4 or RGS14 positive neurons and displaying extensive biocytin filling/ conjugated streptavidin staining, where the entire primary apical dendrite and considerable secondary apical dendrites were visible, were included in this study. The SR/SLM border was determined, by visual examination of the hippocampus under low magnification (10X), by the greater density of the SLM vs. the SR. Images were analyzed with Imaris image analysis software (Bitplane, Concord, MA) for morphometrics and Neurolucida 360 software (MBF Bioscience, Williston, VT) for neuronal tracing.

Primary apical dendrite length was determined by measuring the distance from the base of the dendrite at the cell body to the point of the first major bifurcation using Imaris image analysis software. Only dendrites with a diameter greater than 3.0 microns were considered 1° apical dendrites. Major 1° apical dendrite bifurcations were identified as having initial branch diameters of 2–3 microns. Secondary apical dendrites were classified as those dendrites less than 3.0 microns in diameter. Total apical dendrite surface area was calculated by Imaris image analysis software. In short, the surface area of measured apical dendrites

was calculated using the following equation: SA (surface area)= $2\pi rl+2\pi r^2$ where r=radius and l=length of each measured segment. Total surface area is the summation of all measured apical dendrite surface areas.

Unsupervised learning/Kmeans clustering.

Cell parameter data for putative Ma-like, Mb-like and Mc-like cells were analyzed using R (v.3.2.2). Data were scaled, but not centered, per parameter, and then the mean of each column was subtracted. The Kmeans and principal component analysis (PCA) were generated using the amap (v. 0.8–14) package and visualized using rgl (v. 0.98.1) and misc3d (v. 0.8–4) packages. Analyses were performed on a subset of the cell morphometric data ("1° Apical Dendrite Length", "2° Branch SLM", and "SR SLM 2° Branch Ratio") and included 3 centers with 20 random start sets with the Pearson method for distance (Lucas, 2014). See supplement for details on Kmeans clustering analysis.

Quantification and Statistical Analysis.

Using a previous study of CA2 pyramidal cell morphologies as a guide (Bartesaghi & Ravasi, 1999), a power analysis was performed to determine the number of cells required for statistical significance using SAS/STAT(R) 14.1 Power Procedure (SAS, Cary NC). With an alpha level of 0.05 and a power level of 80%, we calculated requiring at least 15 cells per group (45 total) for statistical significance. Either Prism 7 (GraphPad Software, La Jolla CA) or JMP Pro 13 (SAS, Cary NC) was used for all other statistical analyses. Results were expressed as mean ± SEM with $p < 0.05$ being considered statistically significant. Statistical tests were carried out using one-way analysis of variance (ANOVA) for figures 3,4, 5A-C, 6, and 8 or simple linear regression for figure 5D. For statistical significance, * ≤ 0.05, ** ≤ 0.01, *** ≤ 0.001.

Results:

Identified CA2 Pyramidal Cells Subtypes have Distinct Morphologies.

Upon visual inspection of high-resolution confocal images of streptavidin-stained mouse CA2 pyramidal neurons, we identified cellular subtypes reminiscent of the four identified in guinea pig (Bartesaghi & Ravasi, 1999) (monoapical Ma-like, Mb-like, Mc-like, and biapical B-like: Figure 1). In comparison to guinea pig, mouse M-like cells had distinct, thick, variable-length single 1° apical dendrites extending from the soma (Figure 1A, 1B) with differential 2° apical dendrite branching patterns. Also similar to guinea pig, we positively identified a single B-like CA2 pyramidal cell type that had two thick 1° apical dendrites extending directly from the soma (Figure 1A, 1B: right). Like in guinea pig, B-like cells in mouse were rare (only 1 of 56 biocytin/streptavidin Amigo2-GFP positive cells was confirmed to be a B cell), so B-like cells were not included in further analysis. Mouse hippocampal pyramidal neurons across CA1 appeared more homogeneous in that they displayed a smaller soma than CA2 pyramidal neurons and possess a single, larger-diameter 1° apical dendrite that terminated in a branching of thin 2° apical dendrites (Figure 1C).

Neuronal tracing of high-resolution confocal images of individual biocytin/streptavidin stained Amigo2-GFP positive mouse CA2 pyramidal neurons allowed us to classify 1° and

2° apical dendrites based on diameter, with 1° dendrites defined as those with diameters >3.0 μm (1°: 3.26 ± 0.14 μm, 2°: 1.76 ± 0.18 μm, n=55 cells, Figure 2A). These differences in diameter were then used as criteria to identify 2° apical dendrite branch points derived either from 1° apical dendrites or from other 2° apical dendrites. Measurements of pyramidal cell 1° apical dendrite lengths, total 2° apical dendrite branch number, SR and SLM 2° apical dendrite branch numbers, 2° apical dendrite branch SR/SLM ratio, and total apical dendrite surface areas (subsequently divided into SR and SLM sub-area measurements as well as SR/SLM apical dendrite surface area) were used to create CA2 pyramidal cell morphometric profiles (Figure 2A, 2B). Total apical dendrite surface area was measured as the area in both the SR and SLM (SR+SLM: Figure 2B). Apical dendrite surface area was then subdivided into SR and SLM areas based on layer boundaries (determined by visual examination of the hippocampus by the greater opaqueness of the SLM vs. the SR. Figure 2B, dashed lines)

Utilizing the 1° apical dendrite length and 2° apical dendrite branch numbers (specifically, 1° apical dendrite length, 2° apical branch number SLM, and 2° apical branch number SR/SLM ratio), we set out to unbiasedly classify each cell into one of the three groups (representing the three M cell subtypes) using Kmeans clustering, an unsupervised machine learning method used previously to identify morphologically-distinct subclasses of CA1 pyramidal neurons in mice (Li et al., 2017). To visualize the Kmeans clustering, we performed a principal component analysis (PCA) with the same subset of the cell morphometric data and colored the three groups based on the Kmeans clustering. As seen in Figure 2C, cells distinctly clustered into groups of 16 (black), 24 (red), and 15 cells (gray).

We next plotted the cells in ascending order according to their measurements of SR/SLM apical dendrite area ratio, 2° apical dendrite branch number in SLM, or 1° apical dendrite length (Figure $2D_{1–3}$, respectively) and color-coded each cell corresponding to the PCA clustering. Each histogram revealed a separation of cells predominantly into two groups. The SR/SLM apical dendrite area ratio plot (Figure $2D_1$) shows 20 cells with a ratio greater than 2.5 (as determined by the value assigned by the PCA as the delineation point between putative cell types: average 4.55 ±0.4, Figure $2D_1$) and 35 less than 1.8 (average 1.28 ± 0.05, Figure $2D_1$). The cells corresponding to the red bars had a distinctive morphometric pattern whereby the primary apical dendrite was shorter, and the majority of the apical dendrite area resided in the SR with little to none extending into the SLM (Mb-like Figure 1A, 1B, Table 1). These cells morphometrically closely resembled the Mb cells identified in guinea pig and are subsequently referred to as Mb-like cells.

Plotting the 2° apical dendrite branch number in SLM (figure $2D_2$) again revealed that the cells could be separated into two general groups. Twenty-five cells had less than 14 apical dendritic SLM branches, 24 of which (as determined by the PCA by the delineation point between putative cell types: average 2.67 ± 0.4, Figure $1D_2$) corresponded to Mb-like cells. Thirty cells fell into a second category with greater number of SLM 2° apical dendrite branches (26.3 ± 1.85, n=31: Figure $2D_2$). Interestingly, this group of cells appeared to have a distinct distribution of cells with medium SLM 2° branch number (gray) and high 2° branch number (black) cells. The morphometric pattern of the cells corresponding to the black bars resembled that of Ma cells identified in guinea pig with shorter apical dendrites

but a high degree of 2° apical dendrite branching in the SLM (Figure 1A, B. Table 1). We refer to these as Ma-like cells in the remainder of the manuscript.

Finally, plotting the cells by length of the 1° apical dendrite and color coding each cell according to the PCA analysis indicated that although Ma- and Mb-like cells had similar 1° apical dendrite lengths (see Table 1), a third group of PCA-identified pyramidal cells, had significantly greater dendrite lengths, which often extended into the SLM (see Table 1; grey bars in Figure 2D). The longer 1° apical dendrite was reminiscent of Mc cells in guinea pig that had significantly longer 1° apical dendrites than either Ma or Mb cells. These cells are referred to as Mc-like neurons.

After establishing the presence of three morphologically distinct cell types, we sought to confirm that 1° apical dendrite lengths as well as 2° apical dendrite branching patterns were different between Ma-, Mb-, and Mc-like cell subtypes. Indeed, primary apical dendrite lengths for Mc-like cells were significantly longer that those of Ma- and Mb-like cells (Figure 3A, Table 1). Total number of 2° apical dendrite branches and 2° dendrite branching in SR were significantly greater for Ma-vs. Mb- and Mc-like cells (Figure 3B, 3C. Table 1). However, Ma-and Mc-like cells showed greater 2° dendrite branching than Mb-like cells in SLM (Figure 3D, Table 1). Consequently, the lack of considerable Mb-like 2° apical dendrite branching in the SLM resulted in a significantly larger SR/SLM 2° apical dendrite branch ratio in Mb-like than either Ma- or Mc-like cells (Figure 3E, Table 1).

We also examined the differences in SR, SLM and total apical dendrite areas between Ma-, Mb-, and Mc-like CA2 pyramidal cell subtypes identified in mouse. We measured total dendritic area for each cell according to its classification and plotted the total areas for each cell according to its designated cell type (Figure 4A). We found that total apical dendritic area was not significantly different between Ma- and Mc-like cells, but Mb-like cells had significantly less total apical dendrite areas than either Ma- or Mc-like cells (Figure 4A, Table 1).

We next separated apical dendrite areas for each cell type into their SR and SLM components using the same boundaries illustrated in Figure 2B. Similar to 2° dendritic branching (Figure 2), we found that Mb-like cells had significantly less apical dendrite surface area in SR than either Ma- or Mc-like cells (Figure 4B, Table 1). SR apical dendrite area was not significantly different between Ma- and Mc-like cells (Figure 4B, Table 1). In accordance with SR 2° apical dendrite branching, SLM area in Mb-like cells was markedly less than SLM area in either Ma- or Mc-like cells (Figure 4C, Table 1). Similar to SR apical dendrite surface area, apical dendrite surface area in SLM was roughly equivalent for Ma- and Mc-like cells (Figure 4C, Table 1). Although both SR and SLM apical dendritic areas for Mb-like cells were comparatively smaller than Ma- and Mc-like cells, the overall ratio of SR to SLM apical dendritic surface area for Mb-like cells was significantly greater than that for Ma- and Mc-like cells (Figure 4D, Table 1). Apical dendritic surface area ratios for Ma- and Mc-like cells were not significantly different (Figure 4D, Table 1).

Apical dendrite morphology is reflected in electrophysiological properties of CA2 pyramidal cells.

Mouse pyramidal neurons differ in their electrophysiological properties across CA1, CA2, and CA3 hippocampal sub-regions, and also vary within each sub-region (Mercer, Trigg, & Thomson, 2007; Sun et al., 2017). The cytological features we observed from CA2 pyramidal neuron apical dendrites suggest that different cell types may have different electrophysiological properties and be engaged differently by excitatory inputs from intra- and extra-hippocampal regions of the mouse brain. Therefore, we next investigated the electrophysiological properties and the ability of cortical and intra-hippocampal inputs to induce excitatory responses in the different CA2 pyramidal cell subtypes. We found that Ma-, Mb-, and Mc-like CA2 pyramidal cell subtypes did not differ significantly in resting membrane potential (Figure 5A, Table 2). However, we did observe differences in input resistance (IR) and capacitance, which were both significantly smaller for Mb-like cells compared to Ma- and Mc-like cells (Figure 5B, 5C, Table 2). Because capacitance often reflects the amount of cellular surface area, we asked whether the total apical dendrite surface area for Ma-, Mb-, and Mc-like cells correlated with capacitance (Figure 5D). As expected, CA2 pyramidal cell capacitance was positively correlated with apical dendrite surface area (Figure 5D) when taking all cell types into account. Mb-like cells, with their smaller apical dendrite surface areas, had lower capacitances compared with Ma-like and Mc-like cells, which have greater apical dendrite surface areas. These data suggest that the lower capacitance of Mb-like cells may be due to their smaller overall dendritic areas.

In an attempt to replicate the findings of Chevaleyre et al., and to determine the relative efficacy of excitatory inputs onto CA2 pyramidal neurons in the SLM and SR, we placed stimulating electrodes into both the SLM and SR in or near CA2 to stimulate inputs from the entorhinal cortex (EC) and Schaffer collaterals, respectively (Figure 6A) (Chevaleyre & Siegelbaum, 2010). We then obtained whole-cell somatic excitatory postsynaptic current (EPSC) recordings from CA2 neurons approximately equidistant from each stimulating electrode. Stimulation in SR evoked EPSCs from all recorded cells over a range of potentials (n=55). EPSCs recorded from identified Ma-like cells (n=16) increased in amplitude as SR stimulus intensity was increased (Figure 6B, Table 2). Similarly, Mb-like and Mc-like cell average EPSC amplitudes increased as SR stimulus intensity increased (Figure 6C and 6D, respectively, Table 2), and the response amplitudes were comparable in all cell types. Focal stimulation of the SLM, however, evoked strong EPSC responses only in Ma- and Mc-like cells (Figure 6B, 6D, Table 2) but not in Mb-like cells (Figure 6C, Table 2). In fact, responses to SLM stimulation in Mb-like cells rarely surpassed 25 pA, even at the highest stimulation intensities (Figure 6C, Table 2). When plotted as a ratio of SR-stimulated EPSC amplitude to SLM-stimulated EPSC amplitude, Mb-like cells had a roughly 2.5 times greater ratio over all stimulus intensities, in contrast to a Ma- and Mc-like cells, which had ratios of approximately 1 across stimulus intensities (Figure 6E, Table 2). The attenuated SLM EPSC amplitude in Mb-like cells is likely due to the significantly smaller SLM apical dendritic coverage and presumably fewer ECII excitatory inputs onto Mb-like cells compared with Ma- and Mc-like cells. In no cells did the EPSCs evoked in SLM exceed those evoked with SR stimulation by more than 10%.

Apical dendrite morphology is reflected in action potential firing in CA2 pyramidal cells.

In a previous study, Sun et al. reported that CA2 pyramidal cell dendrites are uniquely suited for transmitting signals from the distal dendrites to the cell bodies to produce action potentials (APs) (Sun et al., 2014). Given our observation of three distinct dendritic structures, we sought to test whether one of these patterns better transmitted signals from the distal synapses than the others and whether APs reflected the EPSCs evoked with SR or SLM stimulation. In order to address this question, we activated these two inputs synaptically with brief stimulus bursts (5 pulses at 100 Hz), using the same stimulating electrode placement in the SR and SLM as above, and measured action potential firing in CA2 neurons. Lower SR and SLM stimulation intensities (20 and 40 μA) triggered AP spikes in 8.3% (1/12) and 25% (3/12) of identified Ma-like cells, respectively (Figure 7A). At higher stimulation intensities (60–100 μA), SR and SLM stimulation both produced depolarizations sufficient to induce APs in up to 100% of the Ma-like cells (Figure 7A). Similar percentages of Mb-like cells responded to SR stimulation over a range of intensities (Figure 7B). However, in contrast to Ma-like cells, the Mb-like cells rarely, if ever, fired action potentials in response to SLM stimulation, even at the highest stimulation intensities (2/11, or 18.2%, of cells at 100 μA; Figure 7B). We expect this is again likely due to the smaller apical dendritic surface area of the Mb-like cells measured in SLM compared to the SR (see Figure 4). Action potentials in Mc-like cells behaved in a way similar to Ma-like cells in that the percentage of responding cells were comparable in response to SR and SLM stimulation over a range of stimulation intensities (Figure 7C). Thus, the similar effectiveness of AP recruitment in response to SLM stimulation in Ma- and Mc-like cells likely reflects the similarity in total dendritic area in SLM (Figure 4C) but not 2° branch number within SLM (with Ma-like > Mc-like cells; Figure 3D). Considering the EPSC results, the SR/SLM ratio of the percent of Ma-, Mb-, or Mc-like cells responding with action potentials was at least 2.5-fold or greater in Mb cells over stimulation intensities ranging from 40–100 pA (Figure 7D).

One factor contributing to the lack of SLM stimulation-induced action potentials in Mb-like cells could be the differences in intrinsic membrane properties of Mb-like cells versus Ma- and Mc-like cells. In order to test for this possibility, we induced somatic action potentials non-synaptically via the whole-cell patch pipette under current clamp using depolarizing pulses at increasing 5-pA intervals and measured a number of action potential parameters. Average action potential threshold for the first induced action potential was not significantly different between Ma-, Mb-, and Mc-like cell types (Figure 8A). Interestingly, though, the amount of current required to induce an action potential response (rheobase current) in Mb-like cells was significantly less than in Ma- and Mc-like cells (Figure 8B, Table 3). Although consistent with the lower cell capacitance and smaller total apical dendritic coverage (Figures 5D and 4A), this result does not fully explain the lack of response to SLM stimulation in the Mb-like neurons. Also, not able to explain Mb-like responses were the individual action potential kinetics such as AP width, rise time, decay and amplitude, which were not significantly different between cell types (Figure 8C-F, Table 3).

Another measure of AP responses that may differ between cell types is spike frequency adaption. This phenomenon, whereby the inter-spike interval gradually increases during a

depolarizing current pulse, has been attributed to inactivation of depolarizing currents and changes in activity-dependent activation of slow hyperpolarizing currents (Benda & Herz, 2003). We measured the intervals between the first to second AP (1st interval), second to third (2nd), third to fourth (3rd), and fourth to fifth (4th) AP spikes. None of these intervals differed between Ma-, Mb-, and Mc-like cells (Figure 8G, Table 3), indicating that spike frequency adaption was unlikely to explain any differences in synaptically-induced firing seen in these cell types.

Discussion:

Previous studies have shown that hippocampal pyramidal cell morphology varies considerably in the different CA sub-regions. As early as 1934, Lorente de Nó observed significant pyramidal cell dendritic heterogeneity in mouse, monkey, and human brain (Lorente de Nó, 1934). More recent studies further describe hippocampal pyramidal neuron subtype morphological and electrophysiological differences based on hippocampal subregion (Ishizuka et al., 1995; Mercer et al., 2007; Srinivas et al., 2017) and within hippocampal subregions (Bartesaghi & Ravasi, 1999; Li et al., 2017; Sun et al., 2017). In this study, we attempted to determine if a heterogeneous population of pyramidal neurons exists in mouse CA2 similar to that in guinea pig, and if so, whether the heterogeneity can result in any consequential physiological properties.

Although morphological classifications have historically been made visually, we instead sought to determine a classification of these distinct subtypes without subjective bias using a modified unsupervised Pearson's correlation machine-learning method initially used to identify distinct morphological CA1 pyramidal subtypes in mice (Li et al., 2017). Utilizing nine neuronal morphological measurements, the algorithm determined that the CA2 neurons clustered into three distinct groups. This delineation was then further validated independently by a Kmeans and PCA of three data subsets from the full Pearson's correlation (PCA, Figure 1E). Principal component analysis colored by the Kmeans clustering groups separated cells into three different subtypes coinciding with the categorization of cells generated by the Pearson's correlation. Our cluster and PCA indicated the presence of three morphologically distinct subtypes of pyramidal cells in mouse CA2 that recapitulated what was reported for guinea pig.

Visual examination of the three CA2 pyramidal neuron populations from postnatal day 30–45 Amigo2 GFP-expressing mice demonstrated a morphological heterogeneity similar to that found in the adult guinea pig (Bartesaghi & Ravasi, 1999). Consistent with this previous work, we were able to identify cell types in mouse CA2 that closely resembled the monoapical (M) and biapical (B) cells described in guinea pig (Figure 1). Like guinea pig CA2 neurons, mouse monoapical cells had a single, large diameter 1° apical dendrite extending from the soma while biapical cells had at least two large diameter apical dendrites extending from the soma. Also similar to the guinea pig study, we found that mouse B cells were very rare, as we were only able to positively confirm one of the fifty-six cells as a B-like cell that was positive for GFP, PCP4, or RGS14. Also similar to guinea pig, there did not appear to be a selective localization of cell types within CA2 in that each mouse CA2

pyramidal cell subtype appeared along the proximal-distal axis within CA2 (data not shown).

Interestingly, our three identified mouse CA2 pyramidal cell subsets were morphologically similar to the monoapical CA2 pyramidal cell subtypes (Ma, Mb, and Mc) Bartesaghi and Ravasi described in guinea pig (Bartesaghi & Ravasi, 1999). Based on apical dendrite morphology, mouse Ma- and Mb-like cells had 1° apical dendrites similar in length but were significantly shorter than Mc-like cells. This observation differed from guinea pig in which Ma cells had distinctly longer 1° apical dendrites than Mb cells. In contrast to mouse Mb-like cells, Ma-like cell 1° apical dendrites frequently ended in a tuft of thinner 2° branches, whereas Mb cells had a distinct bifurcation into two short, thick trunks which then rapidly tapered into thinner 2° apical dendrite branches (Figure 1A, 1B). Mouse Ma-like cells also differed from Mb-like cells in that Ma-like cell apical dendrites extended into SLM, whereas Mb-like cell apical dendrites appeared to be primarily limited to the SR (Figure 1B). More similar to guinea pig, mouse Mc-like cells had longer 1° apical dendrites compared to Ma- and Mb-like cells and also had significant apical dendrite area in the SLM, similar to Ma-like cells but different from Mb-like cells (Figure 1B). Plotting the 1° apical dendrite length, 2° apical dendrite branching, total apical dendrite area, and SR/SLM apical dendrite area ratio versus cell number substantiated the observation of the presence of different Ma-, Mb- and Mc-like monoapical cell types morphologically (Figure 3). Of note is that the overall 1° apical dendrite lengths in mouse were nearly twice that found in guinea pig indicating that there may be some significant differences in M-cell parameters across species.

Similar to 1° apical dendrite length, total apical dendrite surface area measurements and subsequent ratios of apical dendrite surface area in the SR versus the SLM again distinguished separate Ma-, Mb- and Mc-like mouse CA2 pyramidal cell subtypes (Figure 4). Of particular interest was that Mb-like cells, while having 1° apical dendrite lengths comparable to Ma-like cells, had notably smaller apical dendritic area in the SLM as opposed to Ma- and Mc-like cells resulting in a significantly higher SR/SLM apical dendrite area ratio (Figure 4B, C, D). The majority of the apical dendrite area in the Mb-like cells resided in the SR, with on average less than 20% of the apical dendritic area in the SLM. Intriguingly, several labeled Mb-like cells had no measurable apical dendritic area in the SLM at all (See Figure 2). In contrast, Ma- and Mc-like cells predominantly had SR/SLM ratios closer to one, indicating a more even distribution of apical dendrites in the SR and SLM.

As might have been expected based on the cytological differences between cell types, the electrophysiological properties of the subtypes, on average, differed as well. All three cell types had similar resting membrane potentials, but Mb-like cells had significantly lower input resistances (IRs) and capacitances than either Ma- or Mc-like cells (Figure 5B-D, Table 2). The smaller overall apical dendritic area of the Mb-like cells, largely due to the lack of significant dendrite extension into the SLM compared with Ma- and Mc-like cells, most likely accounts for these differences in IR and capacitance observed (Figure 4A, Table 1).

Like CA1 and CA3, CA2 hippocampal pyramidal neurons receive excitatory input from a variety of extra- and intra-hippocampal sources. CA2 pyramidal neurons have been shown to receive excitatory input from mossy fibers from the dentate gyrus (DG) and Schaffer collaterals (SCs) from CA3 that form synapses primarily onto proximal apical dendrites in the stratum radiatum (Lorente de Nó, 1934). CA2 neurons also receive excitatory synaptic input on more distal apical dendrites localized in the SLM from Cajal-Retzius cells originating within the hippocampal formation (HF) (Anstotz et al., 2016; Anstotz, Lee, Neblett, Rune, & Maccaferri, 2018) as well as outside the hippocampus from hypothalamic supramammillary nucleus (SuM) (Borhegyi & Leranth, 1997; Kocsis & Vertes, 1994; Magloczky et al., 1994) and entorhinal cortex (EC) layer II neurons (Chevaleyre & Siegelbaum, 2010; Kohara et al., 2014; Srinivas et al., 2017). Activation of SC or EC inputs onto CA2 pyramidal neuron apical dendrites via stimulating electrodes placed in either the SR or SLM, respectively, revealed differences in relative effectiveness of synaptic input in Mb-like cells. Excitatory post-synaptic current (EPSC) amplitudes evoked with SR or SLM stimulation were similar in Ma- or Mc-like cells (Figure 6B, D). However, in contrast, Mb-like cells were much less responsive to SLM stimulation, compared with the Ma-or Mc-like cells (Figure 6C). This phenomenon was reflected in the ability of either SR or SLM stimulation to evoke somatically recorded action potentials (Figure 7A, C); Mb-like cells, were rarely capable of generating action potentials in response to SLM stimulation. These differences in the ability of SR and SLM stimulation to induce EPSCs and APs in Mb-like cells was most likely due to the relative lack of apical dendrites in the SLM compared to Ma- and Mc-like cells, in that somatic action potentials induced non-synaptically with current injection revealed no significant differences between AP amplitude, threshold, width, or rise and decay times between cell types (Figure 8 A, C-F). Of note, however, the current required to elicit an action potential (rheobase current) was significantly less in Mb-like cells as opposed to Ma- and Mc-like cells (Figure 8B). This indicates that the lower cell capacitance, likely due in part to the smaller total apical dendritic coverage, does not explain the lack of Mb-like cell response to SLM stimulation. Also, spike frequency adaption, a phenomenon attributed to changes in activity-dependent activation of slow hyperpolarizing currents and inactivation of depolarizing currents (Benda & Herz, 2003), was also indistinguishable between Ma-, Mb-, and Mc-like cells (Figure 8F). These data indicate that the differences seen during SLM-stimulated EPSC and AP responses are best explained by differences in apical dendrite morphology and not intrinsic properties of each cell type.

The differences observed in apical dendrite morphology in mouse CA2 pyramidal neurons may significantly influence overall hippocampal function. The fact that certain CA2 pyramidal neurons receive excitatory input from both the DG-CA3-CA2 intra-hippocampal pathway as well as extra-hippocampal cortical regions such as EC layer II, while other cells do not raises a number of important questions. Previous reports have noted that EC inputs provide a strong excitatory drive to CA2 pyramidal neurons via synapses onto distal dendrites in the SLM and can undergo LTP (Chevaleyre & Siegelbaum, 2010; Kohara et al., 2014; Sun et al., 2014). In contrast, Schaffer collateral inputs to CA2 were reported to be relatively weak, are dominated by strong feed-forward inhibition, and do not readily induce synaptic plasticity (Chevaleyre & Siegelbaum, 2010; M. Zhao et al., 2007). Interestingly, our data fail to support the conclusion that synapses in SLM are more effective than those in SR,

in any of our cell types, measured either with excitatory currents or action potential recruitment (Chevaleyre & Siegelbaum, 2010; Sun et al., 2014). We note that even in the Ma- and Mc-like neurons, stimulation in the SLM and SR were comparable in their effectiveness, similar to what was reported by Piskorowski and Chevaleyre (Piskorowski & Chevaleyre, 2013). Although it is certainly possible that different angles of slice cutting could account for the differences between labs, we do not believe that the Mb-like characterization (and lack of response to SLM stimulation) was due to any severing of the distal dendrites; we confirmed that our Mb-like cell dendrites were not abutting the edge of the slices. At present, however, our data cannot explain why some preparations seem to favor the SLM synapses over those in SR (Chevaleyre & Siegelbaum, 2010; Sun et al., 2014).

With the differential signaling strength from CA3 and EC, what is the significance of one subtype of CA2 pyramidal cells ability to respond to both Schaffer collateral and EC stimulation while the other subset only responds to SC input? Also, do certain CA2 pyramidal cell subtypes selectively project to one region of the brain while another subset projects to another region providing a preferential forward signaling depending on the source of excitatory drive into CA2? Interestingly, a recent report described a population of CA2 neurons that appeared to fire in a way that was negatively correlated with sharp-wave ripples, suggestive of at least one distinct functional phenotypes (Kay et al., 2016). CA2 pyramidal neurons have been shown to send axonal projections to CA1 and CA3, as well as back upon CA2 itself and to several extrahippocampal targets including the lateral septum (Cui et al., 2013; Shinohara et al., 2012). Thus, specific CA2 cell subtypes may project differentially to distinct areas, and so certainly warranting further study. As more evidence indicates that CA2 is a critically important hippocampal region involved in social memory processing (Alexander et al., 2016; Hitti & Siegelbaum, 2014), a better understanding of what and how excitatory inputs shape CA2 function is needed.

Supplementary Material

Refer to Web version on PubMed Central for supplementary material.

Acknowledgements:

This research is supported by the Intramural Research Program of the U.S. NIH, National Institute of Environmental Health Sciences (Z01 ES100221 to S.M.D.). We wish to thank members of the Dudek lab, in particular Georgia Alexander, for critical review of this manuscript.

FUNDING: This research is supported by the Intramural Research Program of the U.S. NIH, National Institute of Environmental Health Sciences (Z01 ES100221 to S.M.D.).

References:

Alexander GM, Farris S, Pirone JR, Zheng C, Colgin LL, & Dudek SM (2016). Social and novel contexts modify hippocampal CA2 representations of space. Nat Commun, 7, 10300. doi:10.1038/ncomms10300 [PubMed: 26806606]

Anstotz M, Huang H, Marchionni I, Haumann I, Maccaferri G, & Lubke JH (2016). Developmental Profile, Morphology, and Synaptic Connectivity of Cajal-Retzius Cells in the Postnatal Mouse Hippocampus. Cereb Cortex, 26(2), 855–872. doi:10.1093/cercor/bhv271 [PubMed: 26582498]

Anstotz M, Lee SK, Neblett TI, Rune GM, & Maccaferri G (2018). Experience-Dependent Regulation of Cajal-Retzius Cell Networks in the Developing and Adult Mouse Hippocampus. Cereb Cortex, 28(2), 672–687. doi:10.1093/cercor/bhx153 [PubMed: 28637318]

Aoyagi Y, Kawakami R, Osanai H, Hibi T, & Nemoto T (2015). A rapid optical clearing protocol using 2,2'-thiodiethanol for microscopic observation of fixed mouse brain. PLoS One, 10(1), e0116280. doi:10.1371/journal.pone.0116280 [PubMed: 25633541]

Bartesaghi R, & Ravasi L (1999). Pyramidal neuron types in field CA2 of the guinea pig. Brain Res Bull, 50(4), 263–273. [PubMed: 10582524]

Benda J, & Herz AV (2003). A universal model for spike-frequency adaptation. Neural Comput, 15(11), 2523–2564. doi:10.1162/089976603322385063 [PubMed: 14577853]

Borhegyi Z, & Leranth C (1997). Distinct substance P- and calretinin-containing projections from the supramammillary area to the hippocampus in rats; a species difference between rats and monkeys. Exp Brain Res, 115(2), 369–374. [PubMed: 9224865]

Chevaleyre V, & Siegelbaum SA (2010). Strong CA2 pyramidal neuron synapses define a powerful disynaptic cortico-hippocampal loop. Neuron, 66(4), 560–572. doi:10.1016/j.neuron.2010.04.013 [PubMed: 20510860]

Cui Z, Gerfen CR, & Young WS, 3rd. (2013). Hypothalamic and other connections with dorsal CA2 area of the mouse hippocampus. J Comp Neurol, 521(8), 1844–1866. doi:10.1002/cne.23263 [PubMed: 23172108]

Dudek SM, Alexander GM, & Farris S (2016). Rediscovering area CA2: unique properties and functions. Nat Rev Neurosci, 17(2), 89–102. doi:10.1038/nrn.2015.22 [PubMed: 26806628]

Hitti FL, & Siegelbaum SA (2014). The hippocampal CA2 region is essential for social memory. Nature, 508(7494), 88–92. doi:10.1038/nature13028 [PubMed: 24572357]

Ishizuka N, Cowan WM, & Amaral DG (1995). A quantitative analysis of the dendritic organization of pyramidal cells in the rat hippocampus. J Comp Neurol, 362(1), 17–45. doi:10.1002/cne.903620103 [PubMed: 8576427]

Kay K, Sosa M, Chung JE, Karlsson MP, Larkin MC, & Frank LM (2016). A hippocampal network for spatial coding during immobility and sleep. Nature, 531(7593), 185–190. doi:10.1038/nature17144 [PubMed: 26934224]

Kocsis B, & Vertes RP (1994). Characterization of neurons of the supramammillary nucleus and mammillary body that discharge rhythmically with the hippocampal theta rhythm in the rat. J Neurosci, 14(11 Pt 2), 7040–7052. [PubMed: 7965097]

Kohara K, Pignatelli M, Rivest AJ, Jung HY, Kitamura T, Suh J, Tonegawa S (2014). Cell type-specific genetic and optogenetic tools reveal hippocampal CA2 circuits. Nat Neurosci, 17(2), 269–279. doi:10.1038/nn.3614 [PubMed: 24336151]

Lee SA, Ferrari A, Vallortigara G, & Sovrano VA (2015). Boundary primacy in spatial mapping: Evidence from zebrafish (Danio rerio). Behav Processes, 119, 116–122. doi:10.1016/j.beproc.2015.07.012 [PubMed: 26238575]

Lee SE, Simons SB, Heldt SA, Zhao M, Schroeder JP, Vellano CP, Hepler JR. (2010). RGS14 is a natural suppressor of both synaptic plasticity in CA2 neurons and hippocampal-based learning and memory. Proc Natl Acad Sci U S A, 107(39), 16994–16998. doi:10.1073/pnas.1005362107 [PubMed: 20837545]

Lein ES, Callaway EM, Albright TD, & Gage FH (2005). Redefining the boundaries of the hippocampal CA2 subfield in the mouse using gene expression and 3-dimensional reconstruction. J Comp Neurol, 485(1), 1–10. doi:10.1002/cne.20426 [PubMed: 15776443]

Lein ES, Hawrylycz MJ, Ao N, Ayres M, Bensinger A, Bernard A, Jones AR (2007). Genome-wide atlas of gene expression in the adult mouse brain. Nature, 445(7124), 168–176. doi:10.1038/nature05453 [PubMed: 17151600]

Leroy F, Brann DH, Meira T, & Siegelbaum SA (2017). Input-Timing-Dependent Plasticity in the Hippocampal CA2 Region and Its Potential Role in Social Memory. Neuron, 95(5), 1089–1102 e1085. doi:10.1016/j.neuron.2017.07.036 [PubMed: 28823730]

Li Y, Xu J, Liu Y, Zhu J, Liu N, Zeng W, Zhang X (2017). A distinct entorhinal cortex to hippocampal CA1 direct circuit for olfactory associative learning. Nat Neurosci, 20(4), 559–570. doi:10.1038/nn.4517 [PubMed: 28263300]

Lorente de Nó Rafael. (1934). Studies on the structure of the cerebral cortex. II. Continuation of the study of the study of the ammonic system. J Psychol Neurol, 46, 113–177.

Lu L, Igarashi KM, Witter MP, Moser EI, & Moser MB (2015). Topography of Place Maps along the CA3-to-CA2 Axis of the Hippocampus. Neuron, 87(5), 1078–1092. doi:10.1016/j.neuron.2015.07.007 [PubMed: 26298277]

Lucas Antoine. (2014). Tools for Clustering and Principal Component Analysis (With Robust method, and parallelized functions). Retrieved from https://cran.r-project.org/web/packages/amap/index.html

Magloczky Z, Acsady L, & Freund TF (1994). Principal cells are the postsynaptic targets of supramammillary afferents in the hippocampus of the rat. Hippocampus, 4(3), 322–334. doi:10.1002/hipo.450040316 [PubMed: 7531093]

Mankin EA, Diehl GW, Sparks FT, Leutgeb S, & Leutgeb JK (2015). Hippocampal CA2 activity patterns change over time to a larger extent than between spatial contexts. Neuron, 85(1), 190–201. doi:10.1016/j.neuron.2014.12.001 [PubMed: 25569350]

Mercer A, Trigg HL, & Thomson AM (2007). Characterization of neurons in the CA2 subfield of the adult rat hippocampus. J Neurosci, 27(27), 7329–7338. doi:10.1523/JNEUROSCI.1829-07.2007 [PubMed: 17611285]

Nasrallah K, Piskorowski RA, & Chevaleyre V (2015). Inhibitory Plasticity Permits the Recruitment of CA2 Pyramidal Neurons by CA3(1,2,3). eNeuro, 2(4). doi:10.1523/ENEURO.0049-15.2015

Oliva A, Fernandez-Ruiz A, Buzsaki G, & Berenyi A (2016). Spatial coding and physiological properties of hippocampal neurons in the Cornu Ammonis subregions. Hippocampus, 26(12), 1593–1607. doi:10.1002/hipo.22659 [PubMed: 27650887]

Pagani JH, Zhao M, Cui Z, Avram SK, Caruana DA, Dudek SM, & Young WS (2015). Role of the vasopressin 1b receptor in rodent aggressive behavior and synaptic plasticity in hippocampal area CA2. Mol Psychiatry, 20(4), 490–499. doi:10.1038/mp.2014.47 [PubMed: 24863146]

Piskorowski RA, & Chevaleyre V (2013). Delta-opioid receptors mediate unique plasticity onto parvalbumin-expressing interneurons in area CA2 of the hippocampus. J Neurosci, 33(36), 14567–14578. doi:10.1523/JNEUROSCI.0649-13.2013 [PubMed: 24005307]

Shinohara Y, Hosoya A, Yahagi K, Ferecsko AS, Yaguchi K, Sik A, Hirase H (2012). Hippocampal CA3 and CA2 have distinct bilateral innervation patterns to CA1 in rodents. Eur J Neurosci, 35(5), 702–710. doi:10.1111/j.1460-9568.2012.07993.x [PubMed: 22339771]

Smith AS, Williams Avram SK, Cymerblit-Sabba A, Song J, & Young WS (2016). Targeted activation of the hippocampal CA2 area strongly enhances social memory. Mol Psychiatry, 21(8), 1137–1144. doi:10.1038/mp.2015.189 [PubMed: 26728562]

Srinivas KV, Buss EW, Sun Q, Santoro B, Takahashi H, Nicholson DA, & Siegelbaum SA (2017). The Dendrites of CA2 and CA1 Pyramidal Neurons Differentially Regulate Information Flow in the Cortico-Hippocampal Circuit. J Neurosci, 37(12), 3276–3293. doi:10.1523/JNEUROSCI.2219-16.2017 [PubMed: 28213444]

Sun Q, Sotayo A, Cazzulino AS, Snyder AM, Denny CA, & Siegelbaum SA (2017). Proximodistal Heterogeneity of Hippocampal CA3 Pyramidal Neuron Intrinsic Properties, Connectivity, and Reactivation during Memory Recall. Neuron, 95(3), 656–672 e653. doi:10.1016/j.neuron.2017.07.012 [PubMed: 28772124]

Sun Q, Srinivas KV, Sotayo A, & Siegelbaum SA (2014). Dendritic Na spikes enable cortical input to drive action potential output from hippocampal CA2 pyramidal neurons. Elife, 3. doi:10.7554/eLife.04551

Wintzer ME, Boehringer R, Polygalov D, & McHugh TJ (2014). The hippocampal CA2 ensemble is sensitive to contextual change. J Neurosci, 34(8), 3056–3066. doi:10.1523/JNEUROSCI.2563-13.2014 [PubMed: 24553945]

Zhao M, Choi YS, Obrietan K, & Dudek SM (2007). Synaptic plasticity (and the lack thereof) in hippocampal CA2 neurons. J Neurosci, 27(44), 12025–12032. doi:10.1523/JNEUROSCI.4094-07.2007 [PubMed: 17978044]

Zhao X, Lein ES, He A, Smith SC, Aston C, & Gage FH (2001). Transcriptional profiling reveals strict boundaries between hippocampal subregions. J Comp Neurol, 441(3), 187–196. [PubMed: 11745644]

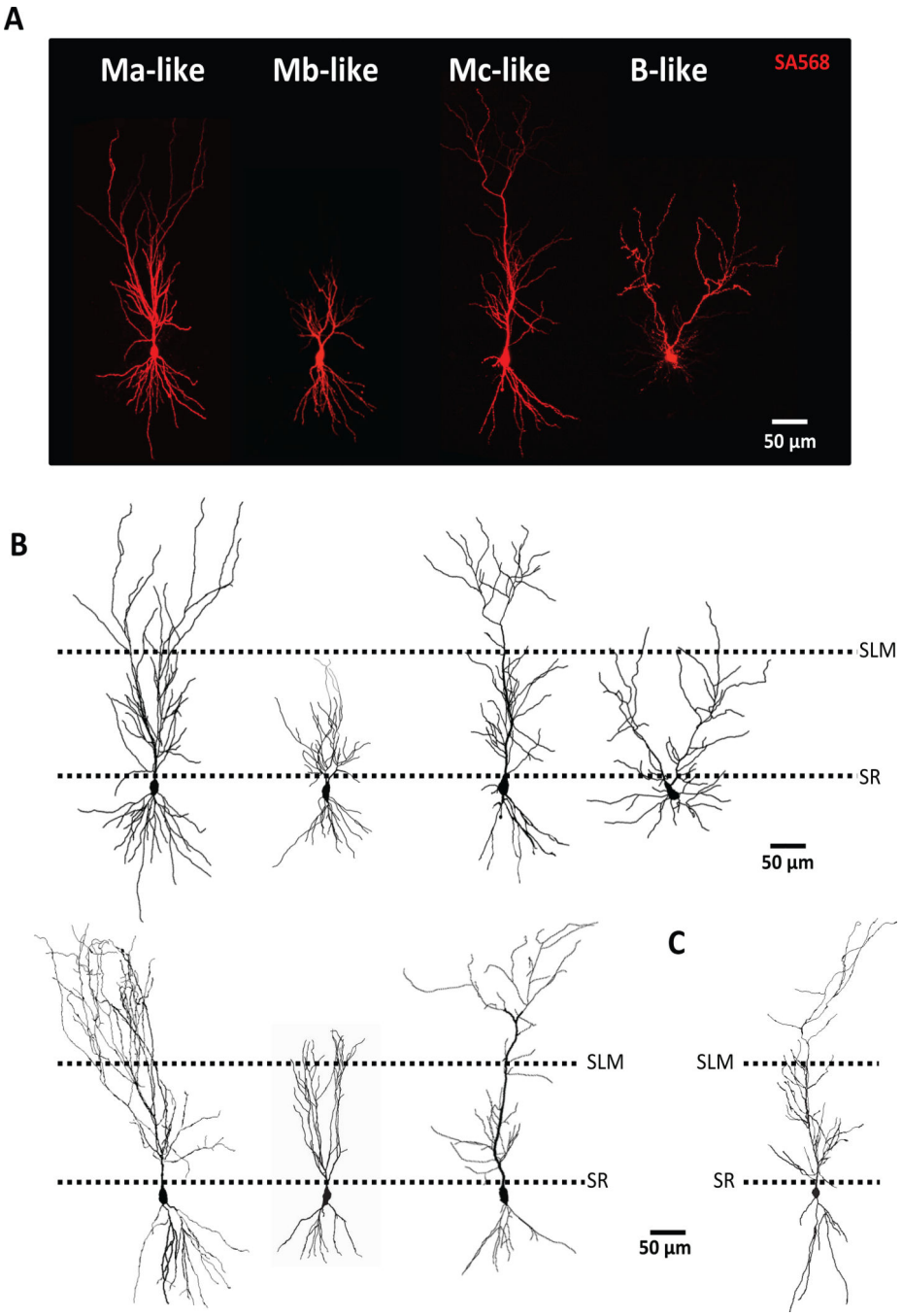

Figure 1.

Confocal images of mouse CA2 pyramidal neurons indicate four possible subtypes. A) Representative confocal images of putative Ma-, Mb-, Mc-, and B-like cells from mouse CA2. B) Neurolucida drawings of representative confocal images from A (top) or other putative Ma-, Mb-, and Mc-like cells (bottom) C) Representative Neurolucida drawing of mouse CA1 pyramidal cell. Border of stratum radiatum (SR) and stratum lacunosum moleculare (SLM) denoted by dashed lines. Scale bar equivalent to 50 µm.

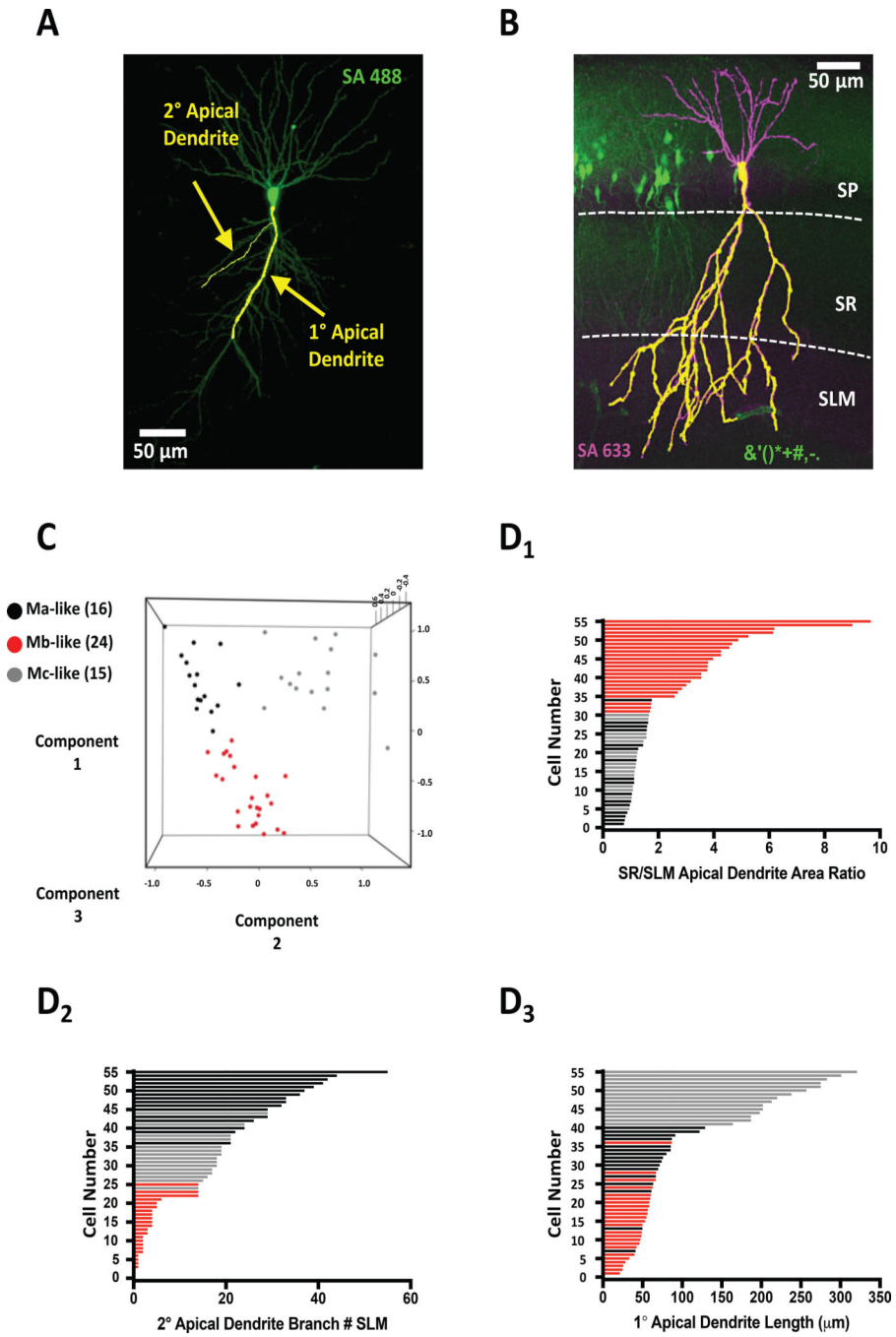

Figure 2.

Unsupervised machine learning reveals three morphologically distinct cell types. A) Representative confocal image of mouse CA2 pyramidal neuron with overlaid Imaris tracing of 1° and 2° apical dendrites. B) Representative confocal image of Amigo2-GFP+ CA2 pyramidal mouse neurons counter-stained with streptavidin (SA633) marking patched, biocytin-filled neuron. Measured apical dendrite area (1° and 2°) denoted by superimposed yellow apical dendritic tracing. Stratum pyramidal (SP), stratum radiatum (SR), and stratum lacunosum moleculare (SLM) layers are denoted by dashed white lines. C) 3D Scatter plot

representing the principal component analysis (PCA) colored by the Kmeans clustering groups. PCA was performed using 1° Apical Dendrite Length (Component 1), 2° Branch SLM (Component 2), and SR SLM 2° Branch Ratio (Component 3). D) Plotting of all Ma-like (black bars), Mb-like (red bars), and Mc-like (gray bars) CA2 pyramidal neurons by either SR/SLM apical dendrite area ratio (D_1), 2° apical dendrite branch number (D_2), and 1° apical dendrite length (D_3). Bar colors correspond to cell-type clusters indicated in PCA in C.

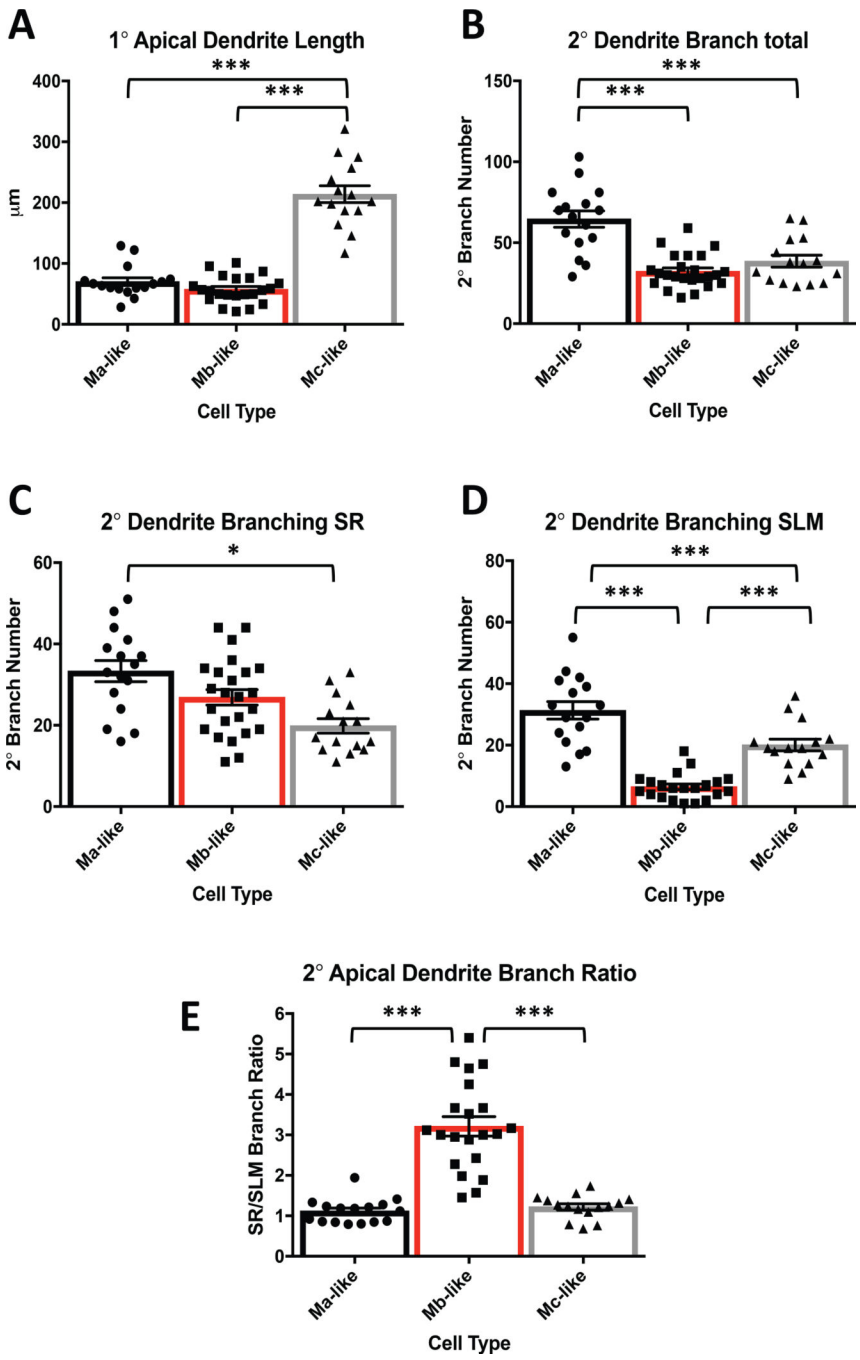

Figure 3.

Distinct CA2 pyramidal cell subtypes have different 1° and 2° apical dendrite characteristics. A) Mc-like cells have significantly longer 1° apical dendrites than Ma-like cells and Mb-like cells (See Table 1 for values. N = 55, F(2, 50)= 101.1, P< 0.0001, 1 way ANOVA). Ma-like and Mb-like cells are not significantly different (Table 1. N = 55, F(2, 50)= 101.1, P= 0.51, 1 way ANOVA). B) 2° apical dendrite branch totals of Ma-like cells are significantly greater than Mb-like and Mc-like cells (Table 1. N = 55, F(2, 52)= 23.78, P< 0.0001, 1 way ANOVA). Mb- and Mc-like cell 2° apical dendrite branch totals were not significantly

different (Table 1. N = 55, F(2, 52)= 23.78, P = 0.41, 1 way ANOVA). C) Ma-, Mb-, and Mc-like cells plotted vs. the number of counted branches in SR. Ma-vs. Mc-like cells were significantly different (Table 1. N = 55, F(2, 52)= 8.425, P = 0.0007, 1 way ANOVA). Ma-like vs. Mb-like, and Mb-like vs. Mc-like are not significantly different (Table 1. P= 0.0826 and 0.0596, respectively). D) Ma-, Mb-, and Mc-like cells plotted vs. the number of counted branches in SLM. Ma-, Mb-, and Mc-like cells are all statistically significantly different from one other (Table 1. N = 55, F(2, 49)= 45.28, P < 0.0001, 1 way ANOVA). E) 2° apical SR to SLM dendrite branch ratios for Ma-, Mb-, and Mc-like cells. Ma-vs. Mb-like and Mb-vs. Mc-like are statistically significantly different (Table 1. N = 55, F(2, 49)= 48.03, P < 0.0001, 1 way ANOVA). Ma- and Mc-like cells are not statistically different (Table 1. N = 55, F(2, 49)= 48.03, P = 0.9175, 1 way ANOVA).

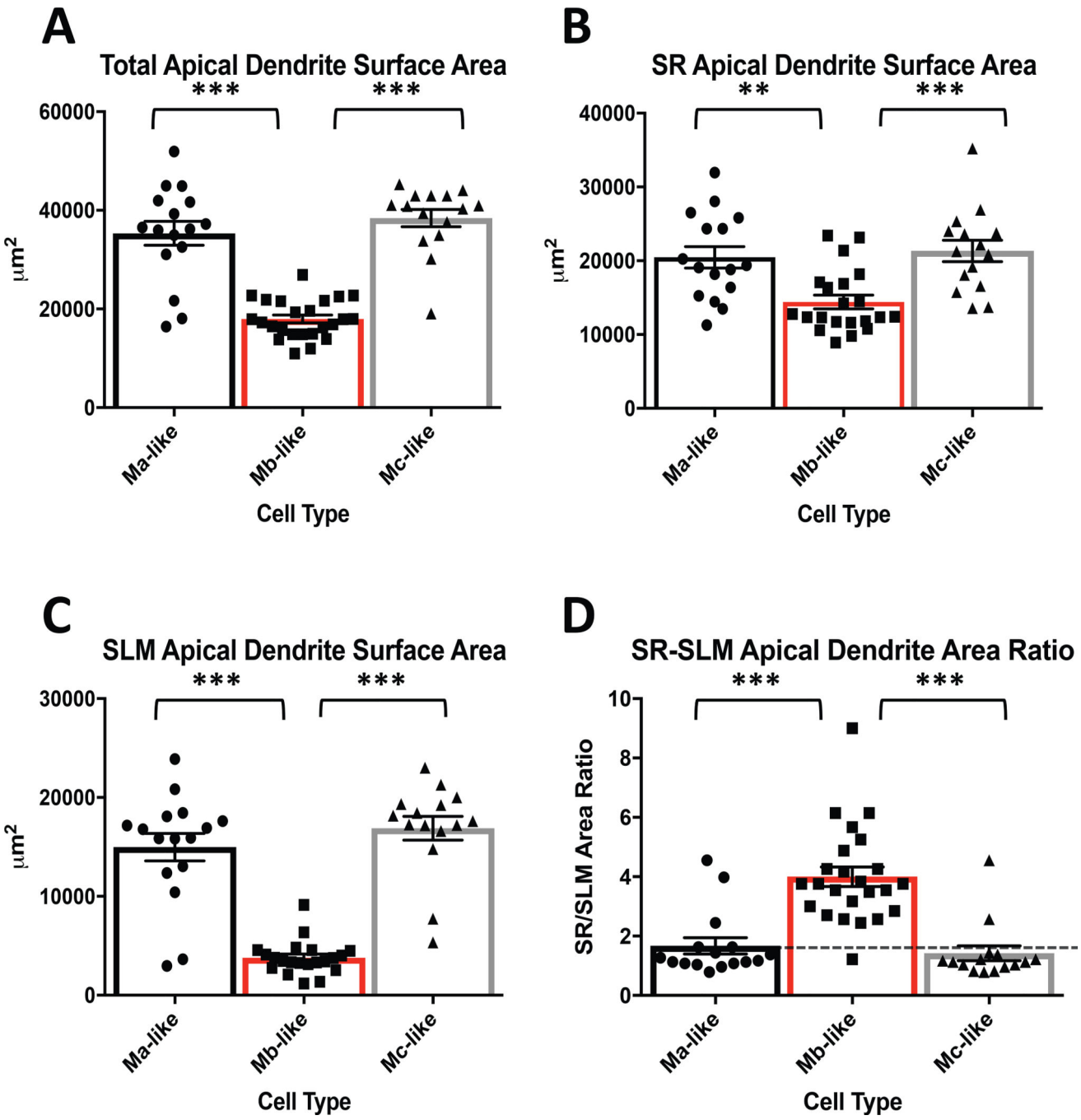

Figure 4.

Comparison of CA2 pyramidal cell apical dendrite areas based on cell type. A) Measured total apical dendrite surface areas for Ma-, Mb-, and Mc-like cells. Ma-vs. Mb-like and Mb-vs. Mc-like cell apical dendrite surface areas are significantly different (Table 1. N = 55, F(2, 52)= 52.5, P < 0.0001, 1 way ANOVA) while Ma-vs. Mc-like are not significantly different (Table 1. N = 55, F(2, 52)= 52.5, P = 0.4223, 1 way ANOVA). B) SR apical dendrite areas for Ma-, Mb-, and Mc-like cells. SR designated as area between stratum pyramidal (SP) and SLM. Ma-vs. Mb-like and Mb-vs. Mc-like are significantly different (Table 1. N = 55, F(2,

49)= 9.913, P = 0.0026 and 0.0007, respectively, 1 way ANOVA). Ma- and Mc-like cells are not significantly different (Table 1. N = 55, F(2, 49)= 9.913, P = 0.8871, 1 way ANOVA). See figure 1B for layer designations. C) SLM apical dendrite areas for Ma-, Mb-, and Mc-like cells. SLM designated as area below SR/SLM boundary (see figure 1B). Ma-vs. Mb-like and Mb- vs. Mc-like SLM apical dendrite areas are significantly different (Table 1. N = 55, F(2, 49)= 55.53, P < 0.0001, 1 way ANOVA) while Ma-vs. Mc-like apical dendrite areas are not different (Table 1. N = 55, F(2, 49)= 55.53, P = 0.4086, 1 way ANOVA). D) SR/SLM apical dendrite area ratio. Ratio based on values from B and C. Dotted line represents 1:1 ratio. Ma-vs. Mb-like and Mb- vs. Mc-like are significantly different (Table 1. N = 55, F(2, 52)= 23.61, P < 0.0001, 1 way ANOVA) while Ma-vs. Mc-like cells are not significantly different (Table 1. N = 55, F(2, 52)= 23.61, P = 0.8569, 1 way ANOVA).

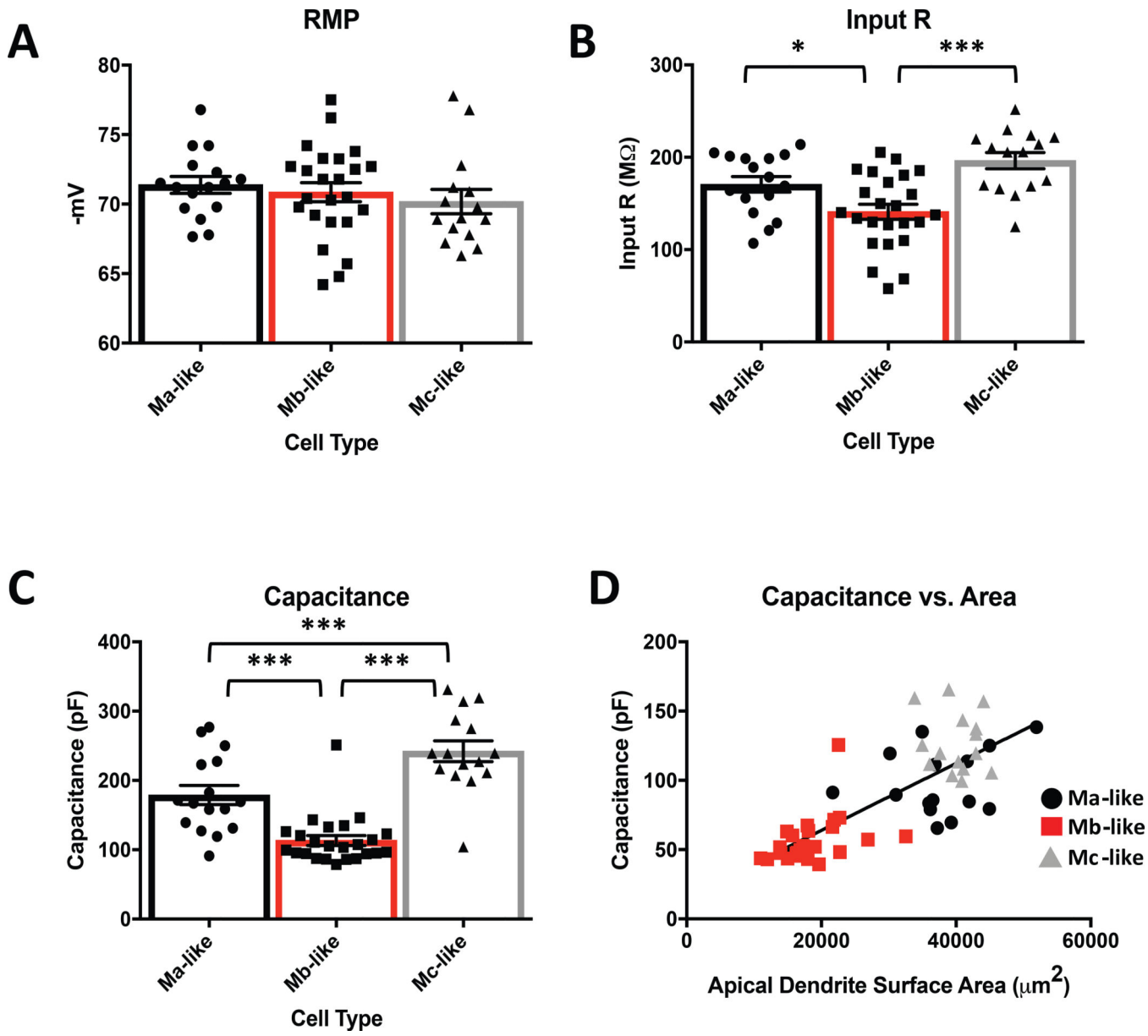

Figure 5.

Passive electrophysiological properties of Mb-like cells differ from Ma- and Mc-like cells. A) Average measured resting membrane potential (RMP) for identified Ma-, Mb-, and Mc-like cells (corrected for liquid junction potential, -10 mV) are not significantly different (Table 2. N = 55, F(2, 52)= 0.5812, P = 0.5628, 1 way ANOVA). B) Average input resistances for Ma-vs. Mb-like cells and Mb- vs. Mc-like cells are significantly different (Table 2. N = 55, F(2, 52)= 10.79, P = 0.0402 and < 0.0001, respectively, 1 way ANOVA) while Ma-vs. Mc-like cells is not significant (Table 2. N = 55, F(2, 52)= 10.79, P = 0.1364,1 way ANOVA). C) Measured average capacitance is significantly different for Ma-vs. Mb-like, Mb- vs. Mc-like and Ma-vs. Mc-like cells (Table 2. N = 55, F(2, 52)= 33.62, P = 0.0003, 0.0017, and < 0.0001, respectively, 1 way ANOVA). D) Linear correlation of

capacitance to measured apical dendritic surface area for Ma-, Mb-, and Mc-like cells ($N = 55$, $F(1, 53) = 78.91$, $P < 0.0001$, simple linear regression).

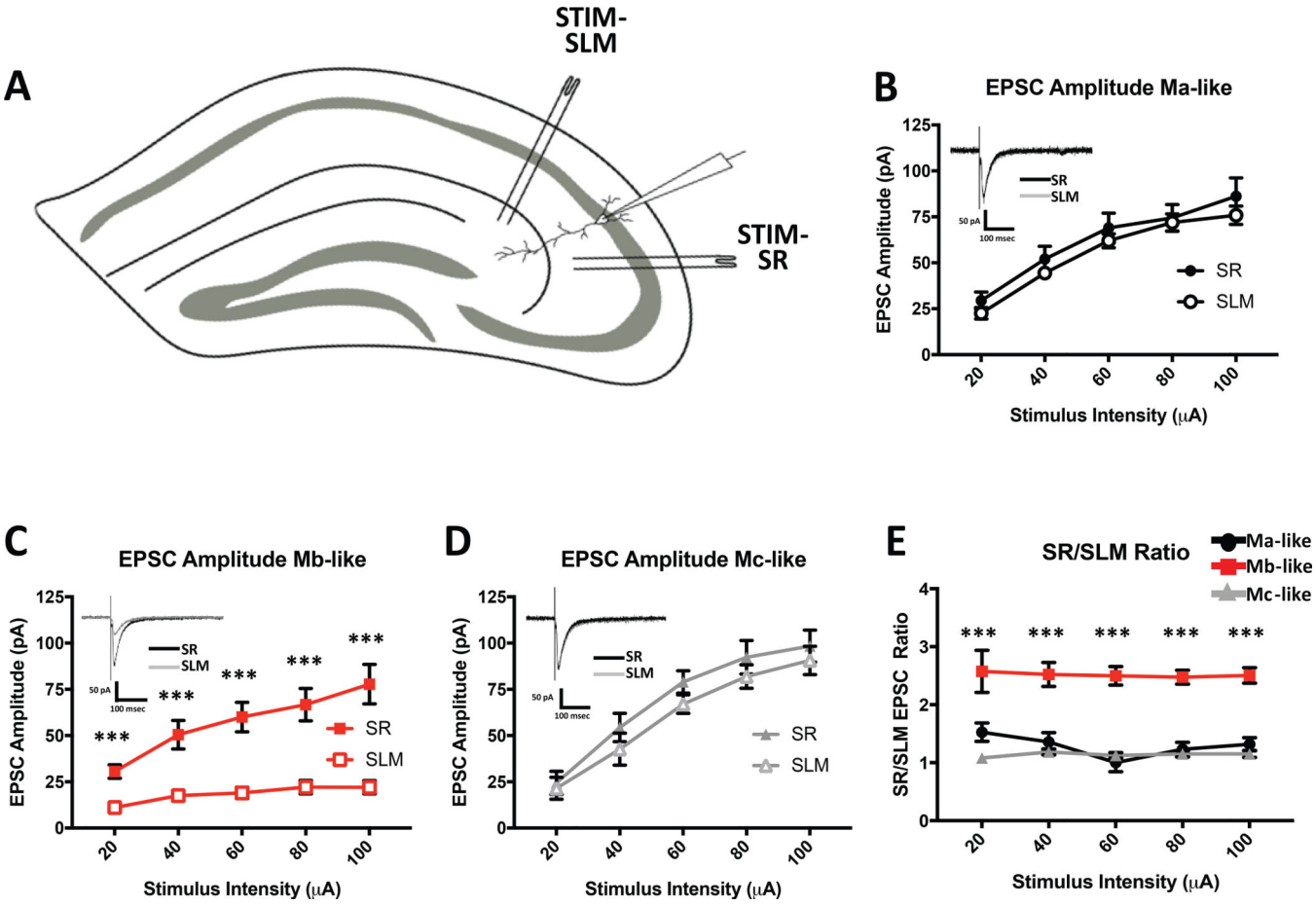

Figure 6.

EPSC amplitudes differ in morphologically distinct CA2 pyramidal cell types. A) Schematic showing the mouse hippocampal slice depicting placement of stimulating electrodes in SR and SLM as well as location of whole cell recording electrode in CA2. B) Average Ma-like cell SR-(closed symbols) and SLM- (open symbols) evoked EPSC amplitudes over 20–100 μA stimulus intensity range. Inset: overlaid representative Ma-like cell SR- (black) and SLM- (gray) evoked EPSC traces from 80 μA stimulus intensity. SR vs. SLM-evoked EPSCs are not significantly different (Table 2. N = 55, P = 0.6360, Unpaired t-test). C) Average Mb-like cell SR- and SLM-evoked EPSC amplitudes over 20–100 μA stimulus intensity range. Inset: overlaid representative Mb-like cell SR (black) and SLM (gray) evoked EPSC traces from 80 μA stimulus intensity. SR vs. SLM-evoked EPSCs are significantly different (Table 2. N = 55, P < 0.0001, Unpaired t-test). D) Average Mc-like cell SR- and SLM-evoked EPSC amplitudes over 20–100 μA stimulus intensity range. Inset: overlaid representative Mc-like cell SR (black) and SLM (gray) evoked EPSC traces from 80 μA stimulus intensity. SR vs. SLM-evoked EPSCs are not significantly different (Table 2. N = 55, P = 0.9006, Unpaired t-test). E) Average ratio of SR- to SLM- evoked EPSC amplitudes for Ma-, Mb-, and Mc-like cells over 20–100 μA stimulus range (Table 2. N = 55, F(2, 52)= 9.399, P < 0.0001, 1 way ANOVA).

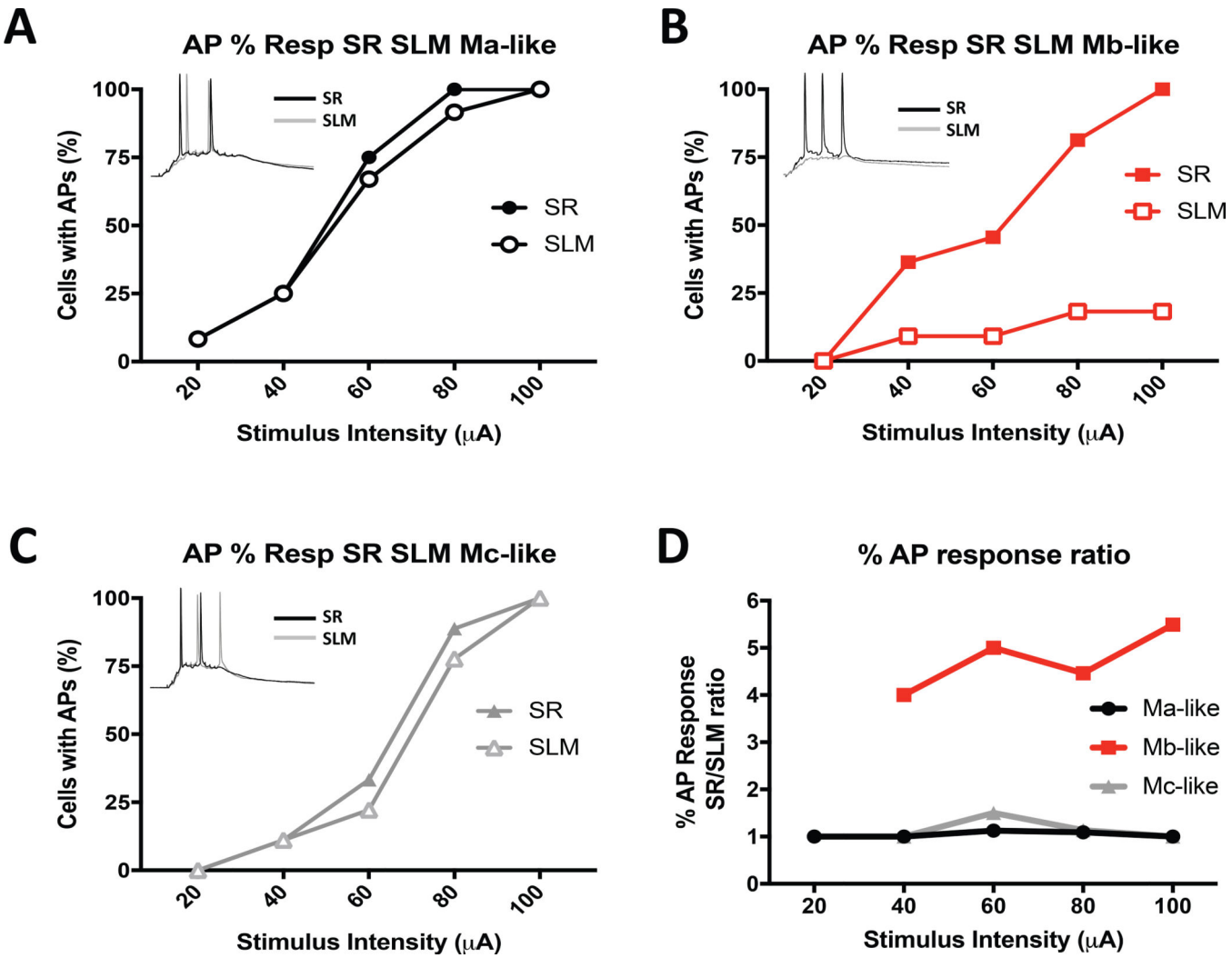

Figure 7.

Effectiveness of action potential recruitment by synaptic stimulation differs in morphologically distinct CA2 pyramidal cells. A-C) Percent of neurons displaying somatic action potentials (APs) in response to a range of stimulus intensities applied to either the SR or SLM for identified Ma-like (A), Mb-like (B) or Mc-like Mc (C) cells. Note that the stimulus consisted of 5 pulses delivered at 100 Hz. Insets: representative action potential traces from either SR (black) or SRM (gray) at 80 μA stimulation. D) Ratios of percentage of cells with stimulated AP responses for Ma- (black), Mb- (red) and Mc-like (gray) cells (taken from A-C).

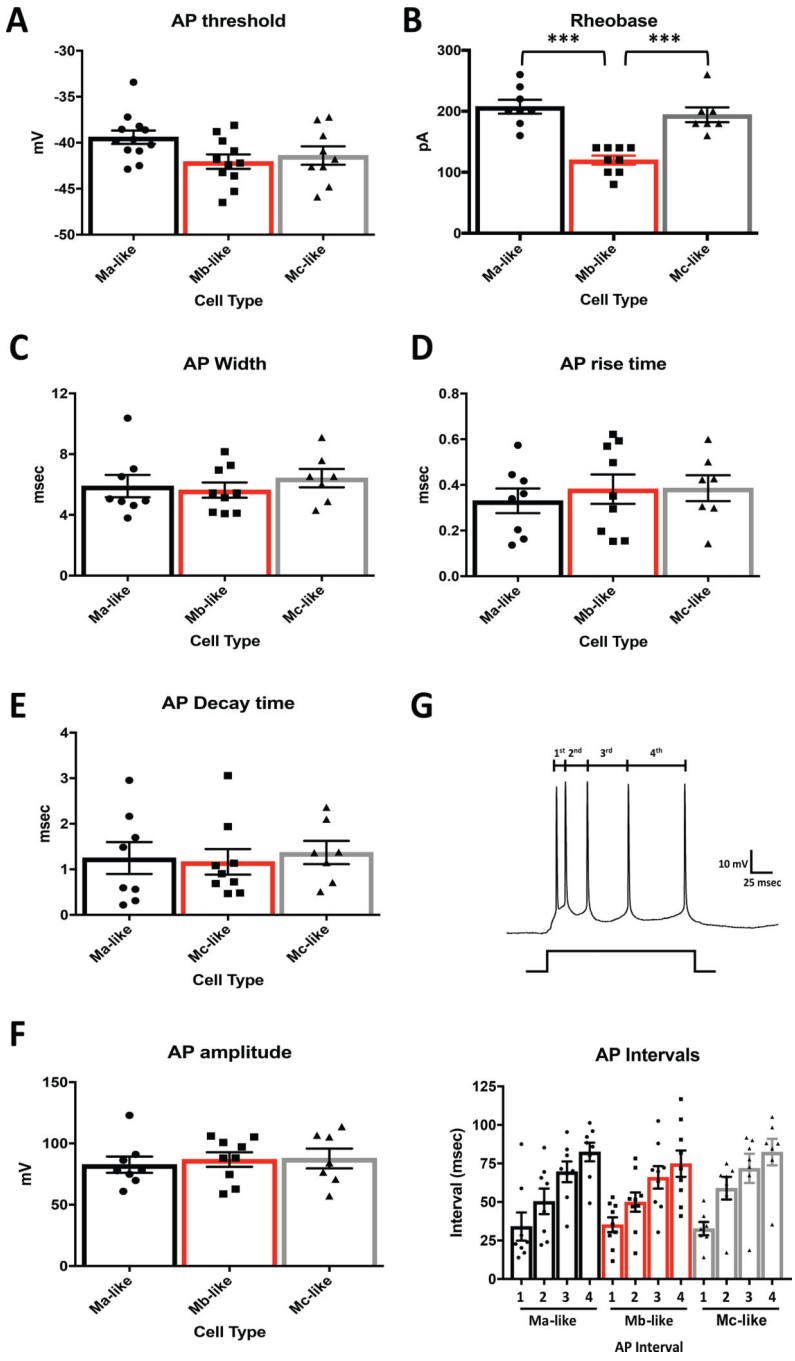

Figure 8.

Action potential kinetics do not differ between CA2 pyramidal cell subtypes. A) Average action potential thresholds for first spike measured in mouse Ma-, Mb-, and Mc-like cells (n=12 Ma-like, n=11 Mb-like, n=9 Mc-like) are not significantly different (N = 32, F(2,29) = 3.044, P = 0.0631, 1 Way ANOVA). B) Average injected current required to induce the first action potential was significantly less for Mb-like cells vs. Ma- and Mc-like cells (N = 32, F(2,21) = 22.95, P < 0.0001, 1 Way ANOVA). Ma-vs. Mc-like cell rheobase measurements were not significantly different (N = 32, F(2,21) = 22.95, P = 0.6530, 1 Way ANOVA). C)

First action potential spike width, measured from the beginning of the action potential rise to the end of the decay, was not significantly different between cell types (N = 32, F(2,21) = 0.4013, P = 0.6745, 1 Way ANOVA). D) Average action potential rise time, measured from the beginning of the action potential rise to the action potential peak, and E) action potential decay time, measured from the action potential peak to the lowest decay point, were also not significantly different between Ma-, Mb-, and Mc-like cell types (N = 32, F(2,21) = 0.2658, P = 0.7691, and F(2,21) = 0.1132, P = 0.8935, respectively, 1 Way ANOVA). F) Average peak amplitudes from induced action potentials were not significantly different between CA2 pyramidal cell subtypes (N = 32, F(2,21) = 0.156, P = 0.8565, 1 Way ANOVA). Peak amplitudes for each generated action potential for individual cells were averaged, and the mean for each cell type is depicted in Figure F. G) Inter-spike durations between induced action potential (AP) spikes. Top: Representative action potentials induced from normal resting potential with current injection and depiction of measured inter-spike intervals. Bottom: Average inter-spike intervals (in msec) between individual induced action potential spikes. Inter-spike intervals for each cell type are not significantly different (N = 32, 1^{st} interval F(2,21) = 0.03826, P = 0.9625: 2^{nd} interval F(2,21) = 0.4473, P = 0.6453: 3^{rd} interval F(2,21) = 0.146, P= 0.8651: 4^{th} interval F(2,21) = 0.3251, P = 0.7260, 1 way ANOVA).

Table 1.

Average morphometric measurements for Ma-, Mb-, and Mc-like cells.

	Ma-like (n=16)	Mb-like (n=24)	Mc-like (n=15)
Apical Dendrite Length/Branching			
1° Apical Dendrite Length (μm)	68.9 ± 6.2	67.3 ± 11.5	214.7 ± 19.2
2° Apical Dendrite Branch #: Total	63.3 ± 5.0	32.5 ± 2.4	41.1 ± 3.9
2° Apical Dendrite Branch #: SR	32.4 ± 2.6	26.0 ± 1.9	22.2 ± 2.3
2° Apical Dendrite Branch #: SLM	30.9 ± 2.7	6.5 ± 0.9	18.9 ± 1.9
2° Apical Dendrite Branch #: SR/SLM	1.1 ± 0.07	3.2 ± 0.2	1.2 ± 0.1
Apical Dendrite Surface Area			
Total Apical Dendrite Surface Area (μm^2)	35436.9 ± 2297.3	17722.3 ± 892.2	38334.7 ± 1543.4
SR Apical Dendrite Surface Area (μm^2)	20454.9 ± 1368.8	14413.7 ± 922.3	21295.2 ± 1282.0
SLM Apical Dendrite Surface Area (μm^2)	14981.9 ± 1301.8	3784.8 ± 370.7	17039.4 ± 1064.1
SR/SLM Apical Dendrite Surface Area Ratio	1.67 ± 0.3	4.56 ± 0.7	1.43 ± 0.2

Table 2.

Average electrophysiological parameters and induced EPSC values for Ma-, Mb-, and Mc-like cells.

	Ma-like (n=16)	Mb-like (n=24)	Mc-like (n=15)
RMP (mV)	−71.5 ± 0.6	−70.6 ± 0.8	−70.4 ± 0.7
Input R (MΩ)	171.7 ± 7.9	139.9 ± 9.2	195.6 ± 7.7
Capacitance (pF)	178.9 ± 13.1	113.3 ± 8.2	244.2 ± 13.2
Ave. EPSC Amp. (SR)			
Stimulus Intensity			
20 μA	29.5 ± 4.5	30.6 ± 3.6	24.4 ± 6.2
40 μA	52.0 ± 7.1	50.5 ± 7.7	54.4 ± 7.7
60 μA	69.1 ± 8.0	60.4 ± 8.2	79.0 ± 6.1
80 μA	74.5 ± 7.3	66.7 ± 8.8	92.4 ± 9.0
100 μA	86.2 ± 10.4	77.8 ± 10.7	98.4 ± 8.7
Ave. EPSC Amp. (SLM)			
Stimulus Intensity			
20 μA	22.5 ± 3.1	11.1 ± 1.9	21.5 ± 5.9
40 μA	44.4 ± 2.3	17.5 ± 2.9	42.7 ± 8.7
60 μA	62.0 ± 3.8	19.0 ± 3.6	67.0 ± 5.2
80 μA	71.9 ± 4.7	22.1 ± 3.1	81.9 ± 6.3
100 μA	75.9 ± 5.0	21.9 ± 3.2	90.6 ± 7.6
SR/SLM EPSC Amp. Ratio			
Stimulus Intensity			
20 μA	1.52 ± 0.16	2.57 ± 0.36	1.08 ± 0.14
40 μA	1.36 ± 0.15	2.52 ± 0.21	1.19 ± 0.15
60 μA	1.01 ± 0.16	2.50 ± 0.16	1.12 ± 0.18
80 μA	1.23 ± 0.12	2.47 ± 0.12	1.15 ± 0.12
100 μA	1.3 ± 0.11	2.56 ± 0.13	1.17 ± 0.16

Table 3.

Average induced action potential metrics for Ma-, Mb-, and Mc-like cells.

	Ma-like (n=8)	Mb-like (n=9)	Mc-like (n=7)
AP Threshold (mV)	−41.2 ± 0.9	−42.3 ± 1.1	−42.8 ± 1.5
Rheobase(pA)	208 ±11.3	120 ± 7.5	194 ± 12.2
AP Width (msec)	5.9 ± 0.7	5.6 ± 0.5	6.1 ± 0.6
AP Rise Time (msec)	0.33 ± 0.05	0.38 ± 0.06	0.39 ± 0.06
AP Decay time (msec)	1.3 ± 0.3	1.2 ± 0.3	1.4 ± 0.2
AP Amplitude (mV)	82.7 ± 6.6	86.9 ± 5.9	87.8 ± 8.0
AP Spike Interval (msec)			
1st	34.1 ± 9.1	35.3 ± 4.8	32.7 ± 4.4
2nd	50.4 ± 8.3	50.0 ± 6.3	58.9 ± 7.4
3rd	69.6± 6.7	66.0 ± 7.3	71.8 ± 9.5
4th	82.5 ± 6.0	74.8 ± 8.5	82.4 ± 8.6